JGR Space Physics

RESEARCH ARTICLE
10.1029/2019JA027164

Nocturnal and Seasonal Variation of Na and K Layers Simultaneously Observed in the MLT Region at 23°S

V. F. Andrioli[1,2,3], J. Xu[1], P. P. Batista[3], A. A. Pimenta[3], L. C. A. Resende[1,2,3], S. Savio[1,2,3], P. R. Fagundes[4], G. Yang[1,2], J. Jiao[1], X. Cheng[5], C. Wang[1], and Z. Liu[1,2]

[1]National Space Science Center, Chinese Academy of Sciences, Beijing, China, [2]China-Brazil Joint Laboratory for Space Weather, NSSC/INPE, São José dos Campos, Brazil, [3]Instituto Nacional de Pesquisas Espaciais (INPE), São José dos Campos, Brazil, [4]IP&D, Universidade do Vale do Paraiba (UNIVAP), São José dos Campos, Brazil, [5]Wuhan Institute of Physics and Mathematics, Chinese Academy of Sciences, Wuhan, China

Abstract The present work shows for the first time the study of morphology of the mesopause sodium (Na) and potassium (K) layers simultaneously observed by a dual-beam LIDAR in the Southern Hemisphere. We analyze these two alkali metal layers from November 2016 to February 2019 measured at São José dos Campos (23.1°S, 45.9°W) and present their nocturnal and seasonal behavior. The night of 25 April 2017 was investigated as a representative of the vertical descending structure frequently observed in the metal density data at this location. We discuss here the chemical and dynamical contribution in the formation of these distinct layers, using simultaneous meteor radar wind and ionosonde data. These downward structures are seen in 66% of Na/K LIDAR data and seem to occur preferentially around April. The good agreement with diurnal tide and the presence of Es layer, suggest a combining mechanism in the formation of these structures. Moreover, semiannual variations are observed in both layers; however, they present different maxima location. The Na density presents its maxima around May and September; whereas, K density shows a strong maximum around July and a weaker one around December. Likewise, semiannual variation with maxima at the equinoxes is observed in the centroid height for both layers. However, the column abundances of these two metals show distinct seasonal variation: Annual variation peaking from one equinox to the other is observed in Na and semiannual with maxima in the solstices in K. The same behavior of centroid height for both layers indicates the same mechanism acting in the seasonal variation, which is not yet completely understood.

Key Points:
- Simultaneous Es layer measured at Cachoeira Paulista and Sao Josedos Campos
- First seasonal analysis of K density by LIDAR in low-latitude Southern Hemisphere
- Semiannual variation observed on Na and K densities, being K behavior similar to Northern Hemisphere measurements

Supporting Information:
- Supporting Information S1

Correspondence to:
V. F. Andrioli,
vania.andrioli@inpe.br

Citation:
Andrioli, V. F., Xu, J., Batista, P. P., Pimenta, A. A., Resende, L. C. A., Savio, S., et al. (2020). Nocturnal and seasonal variation of Na and K layers simultaneously observed in the MLT Region at 23°S. *Journal of Geophysical Research: Space Physics*, *125*, e2019JA027164. https://doi.org/10.1029/2019JA027164

Received 16 JUL 2019
Accepted 20 FEB 2020
Accepted article online 25 FEB 2020

1. Introduction

All the time the Earth's upper atmosphere is reached by cosmic dust particles at very high velocities (11–72 km s^{-1}) and energetic collisions with air molecules cause flash heating until the particles melt and their minerals constituent vaporize (Plane et al., 2015, and references therein). This process leads to the formation of distinct metal atom layers such as sodium (Na), potassium (K), iron (Fe), calcium (Ca), magnesium (Mg), or nickel (Ni). The density of neutral K atoms is difficult to measure in the upper atmosphere, because they are scarce there, being its column abundance around two orders of magnitude smaller than that of Na, 30 versus 800 ($\times 10^7$ cm^{-2}) as observed by Megie et al. (1978). We can say that the studies about Na layer in the mesosphere and lower thermosphere (MLT) region started on the 1930s, when Slipher (1929) first recorded the Na D lines in airglow spectra. About 30 years later, Sullivan and Hunten (1962) obtained the first quantitative identification of the K (D_1) line also in the airglow. Na and K at MLT region were expected to have similar variations as both are from the same chemical group, alkali metals; however, based on LIDAR technique, some works in different latitudes showed that they have distinct seasonal variation and night processes (e.g., Eska et al., 1998; Jiao et al., 2015; Plane et al., 2014; Swider, 1987; Yue et al., 2016, and references therein). Annual variation with maximum in the winter is observed in Na column abundances (e.g., Eska et la., 1998; Simonich et al., 1979); whereas semiannual oscillation with maxima at the solstices is observed on K (Eska et al., 1998; Wang et al., 2017; Yue et al., 2016). Unfortunately, almost all of these studies were conducted at middle or high latitudes in Northern Hemisphere. At Southern Hemisphere, the studies were focused on Na layer alone (e.g., Clemesha et al., 1982; Clemesha & Batista, 2003; Pimenta et al., 2004; Simonich et al., 1979), and only sporadic measurements for K (Eska et al., 1999) have been reported. Atmospheric chemical models (Dawkins et al., 2015; Delgado et al., 2012;

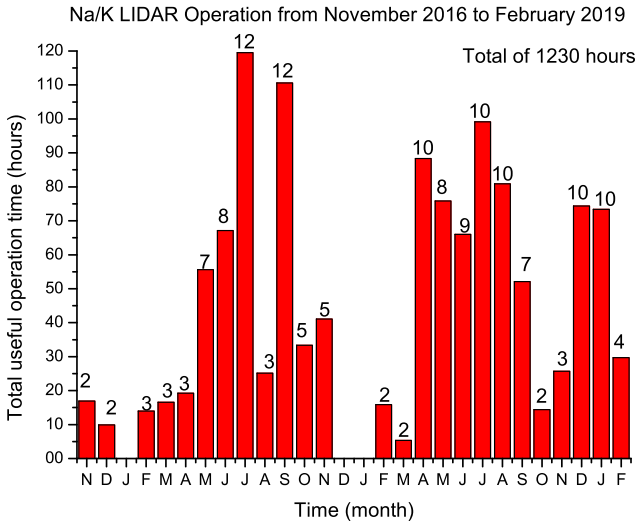

Figure 1. Histogram showing the total monthly hours of Na/K LIDAR data analyzed from November 2016 to February 2019. On the top of each column is shown the number of nights of observation on that month.

Plane, 2003; Plane et al., 2014, and references therein) have helped in the understanding of those seasonal differences, but still disagree with respect to the latitude dependence and total abundance of these alkali metals, as will be discussed in the present work.

We present in this paper the first ground-based simultaneous observation of nocturnal and seasonal variation of Na and K layers measured at Southern Hemisphere. In section 2 we describe the method used to retrieve Na and K densities from LIDAR photon counting. In section 3 we present the results about the nocturnal and seasonal variations of both layers. For a better characterization of the nocturnal layers' morphology, we use simultaneous measurements of meteoric wind radar data and the ionospheric data from two ionosondes away from each other by about 100 km. In section 4 we compare and discuss our results with the previous works. Finally, in section 5 we present the summary and conclusion.

2. Method

A dual beam Na/K LIDAR was installed at São José dos Campos (23.1°S, 45.9°W, thereafter SJC), Brazil on 20 November 2016. Based on resonance fluorescence scattering mechanism and using two laser beams centered at 589 and 770 nm, this LIDAR can obtain simultaneous measurements of Na and K atoms signals from the MLT region. Details of the system and data acquisition can be found in Jiao et al. (2015, 2017).

This LIDAR provides Na and K photon counts with time and height resolution of 20 s and 96 m, respectively. We remove the background noise by using the average number of photons echoes received within 120–130 km height range. In order to increase the signal-to-noise ratio we combine 10 temporally consecutive profiles, with a resulting temporal resolution of 3.3 min when inferring Na and K densities within the MLT region. Using these enhanced profiles and applying the LIDAR equation (1), Na/K number density ($N_{Na/K}$) profiles are obtained.

$$N_{Na/K}(r) = \frac{(n_{Na/K}(r) - n_B)\sigma_R(Na/K)}{(n_R(r_R) - n_B)\sigma_{eff}(Na/K)} \cdot \frac{4\pi N_R(r_R) r^2}{r_R{}^2} \quad (1)$$

Where r is the distance between scattering object and LIDAR receiving system, r_R is the reference height (~45 km), $n_{Na/K}$ is the photon counts of K or Na atoms, n_R is the respective photon count at the reference height, $N_R(r_R)$ is atmospheric number density at reference height from NRLMSISE-00 (2017) model, n_B is respective background noise of each wavelength, σ_{eff} is the effective fluorescence scattering cross section of K or Na atoms and $\sigma_R(Na/K)$ is the Rayleigh scattering cross section for respective wavelength.

Scattering of aerosol particles can be neglected at these altitudes, optical thickness is less than 0.01; the line width of Na and K laser is ~1.473 and 1.77 GHz, respectively; the effective scattering cross section ($\sigma_{eff}(Na/K)$) of Na and K atoms are ~5.22×10^{-16} and $3.29 \times 10^{-17} m^2\ sr^{-1}$, respectively (Jiao et al., 2015, and references therein).

The Na/K LIDAR has been operating since 20 November 2016, totaling 208 nights and more than 1,300 hr of observation up to 28 February 2019. However, in the present work, we have analyzed only the nights with at least 3 hr of data, so the number of analyzed nights reduced to 152, totaling 1,230 hr of observation from November 2016 to February 2019. A histogram showing the total monthly hours of observations and the number of nights for the corresponding month is shown in Figure 1. We note that most part of the observation occurs from May to September. This variation occurs because the system operates only in clear sky weather conditions, so this figure reflects the weather conditions at SJC, where the summer is very wet and the winter is dry. Hence, it is very difficult to have a clear sky in January, for example. Fortunately, there were few cloudy nights in the last summer, and we had plenty of data during December 2018 and January 2019, almost the same number of nights of observation as in the winter. This helps us to have a satisfactory data representative of individual months allowing the seasonal analysis of the morphology of each layer.

3. Results

3.1. Nocturnal Variation on the Layers

The height time intensity of K and Na densities profiles are shown in Figures 2 and 3, respectively, observed on 25 April 2017. A maximum concentration of K density is observed at around 94 km in a thin layer of about 2 km width and lasting for 36 min beginning at 18:30 LT. This strong thin layer is a neutral sporadic (Ns) K layer and shows a time decay behavior until around 2:00 LT. At around 19:00 LT it starts a second upper layer, around 103 km, with its peak altitude also having a downward movement up to around 00:00 LT. This layer connects with the main layer at around 02:00 LT when both layers have steady vertical movement until end of the night. In Figure 3 is shown the Na layer behavior on the same night, and we clearly note the similarities between both these layers morphologies. Although Na concentration shows a wider layer than K, both present the downward movement, from 18:30 LT to 02:00 LT, and layer bifurcation around 00:00 LT. Even though we are presenting here a case study, this downward movement and layer bifurcation are commonly observed in the nighttime Na and K densities profiles measured at SJC. This behavior agrees with the ones observed in the Na layer since the first measurements of Na in SJC with smaller time and height resolution (Kirchhoff & Clemesha, 1973; Batista et al., 1985, 1989). The night of 25 April 2017 has almost 12 hr of observation from 18:30 LT to 6:00 LT allowing us to study the behavior of these two metal layers all night long. Therefore, we will present a deep study over this date, which is a representative Na/K layers nocturnal downward behavior and after all, a statistical analysis over all the data observation is presented in order to better characterize the joint nocturnal variation of Na and K density layers.

The variation of the height peak densities is shown in Figure 4. We infer the rate of these layers decay as 0.96 and 1.02 km/hr, for Na and K, respectively. These rates are in accordance with the diurnal tidal phase movement, around 1 km/hr.

The black line in Figure 5 shows the total column density of K atoms (a) and Na (b). We can observe that the K total column density has larger variability throughout the night than Na. At the beginning of the night, most of the K atoms are in upper altitude, above 90 km (red curve). Subsequently, the column abundance over 90 km decreases and the one between 80 and 90 km (orange curve) increases its amount. However, after midnight, the amount of K in these two layers is almost the same. On the other hand, Na column density remains in the same altitude throughout the night, having most part of atoms above 90 km. In addition, we can observe that the total densities increase their amount about 50% and 16%, for K and Na, respectively, after 00:30 LT. Moreover, these increases can be seen not only on the upper part of the layer (red curve) but also on the bottom (orange curve). This leads us to believe that perhaps there is an input of new atoms in the upper layer, and the presence of strong tidal winds could have driven these atoms to lower altitude increasing the population of K in the layer lower than 90 km. In other words, it means that the bifurcation on the layers, noted in Figures 2 and 3, should be due to not only the input of new atoms from a source but also a relocation of the preexisting atoms due the presence of atmospheric waves such as tides. The tide-induced oscillations in the atmospheric sodium layers were amply discussed by Clemesha et al. (2002) using simultaneous LIDAR and meteor radar winds over SJC.

Figure 6 shows the zonal and meridional winds measured by all-sky meteor radar at Cachoeira Paulista (23°S, 45°W, thereafter CXP), about 100 km away from LIDAR site during the night of 25 April 2017. The strong presence of the tides is noted on these winds profiles, which suggest wave interaction with the Na and K layers. Monthly mean tidal amplitude and phases using days of observation for the month of April 2017 are shown in Figure 7. We can note in panel (a) that diurnal tide reaches 40 ms^{-1} and 75 ms^{-1}, respectively, for zonal and meridional wind. On the other hand, the amplitudes of the semidiurnal tide, shown on panel (c), are much weaker, reaching 20 $ms^{-1}$for meridional wind. Moreover, the phases of these tides are presented on panels (b) and (d) for diurnal and semidiurnal, respectively. We can infer the vertical wavelength of the diurnal tide as 28 km, which corresponds to the (1,1) mode of propagating wave. Therefore, the predominant wind in this region is the first propagating mode of the diurnal tide.

Another interesting feature on this night is the presence of sporadic E (Es) layer throughout almost all night long, as can be observed in ionosonde data shown in Figure 8. In this figure are presented the ionosonde data measurements at SJC, on the upper panels, and CXP, panels on the bottom, on 25 and 26 April 2017. Over CXP, the ionosonde is a Digisonde DPS4D that operates continuously and takes echoes from different altitudes of the ionosphere (ionograms) every 10/15 min. This instrument has a frequency step of 0.5 MHz and a height resolution of ±5 km. In the Digisonde's ionograms (Figure 8b), the overhead reflections for

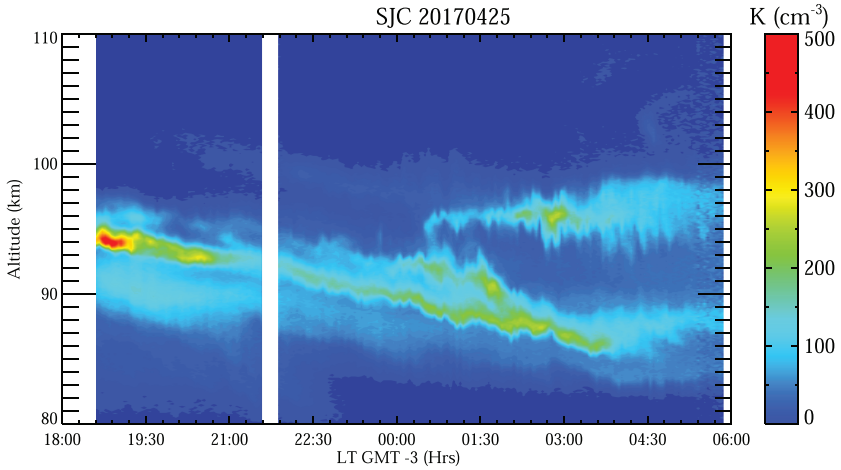

Figure 2. Height time intensity plot of K density layer on 25 April 2017 at São José dos Campos.

ordinary and extraordinary waves are represented as red and green echoes, respectively. The other colors in the ionograms represent off-vertical reflections and are indicative of irregularities in the reflecting layer (Reinisch, 1986). On the other hand, over SJC, the ionosonde used is a CADI (Canadian Advanced Digital Ionosonde). This ionosonde also produces ionograms every 5/10 min. having a frequency step of 2.0 MHz and a height resolution of ±3 km. The colors in the CADI's ionograms, Figure 8a, refer to the amplitude of the signal received (in dB), being the yellow, green, and blue colors representative of the greatest amplitudes (MacDougall et al., 1995). It is possible to note a strong Es layer, identified in the figure by red arrows, since the beginning of LIDAR observation around 18:00 LT on both ionosondes. This Es layer is blocking almost completely the radio frequencies signal from the ionospheric F region up to 19:40 LT. This first Es layer lasts up to 20:40 LT. At around 02:40 LT, on 26 April 2017, another Es layer appears and remains up to the sunrise, reaching higher frequencies. The time evolution of the Es layer is presented in the supporting information. In addition, we have plotted the virtual height (h'Es) of these Es layers at these two sites, in Figure 9. We can see that the altitude (h'Es) of the Es layer observed at SJC is higher than that observed at CXP. The differences between the h'Es measured at SJC and CXP can be related to the resolution of these two Ionosondes. Several observations show that Es and Ns layers often coexist, (Clemesha, 1995; Clemesha et al., 1979; Zhou et al., 2008) and both of them descend frequently at the phase speed of the diurnal tide (Zhou et al., 2005). This close relation between Ns and Es suggests that Es may act in some way as a reservoir for the Ns layer (Delgado et al., 2012). Studies using models and laboratory analysis have also suggested that in the MLT region metal ions in a plasma layer could be neutralized to form Ns metal layers, via dissociative electron recombination (Collins et al., 2002; Cox &

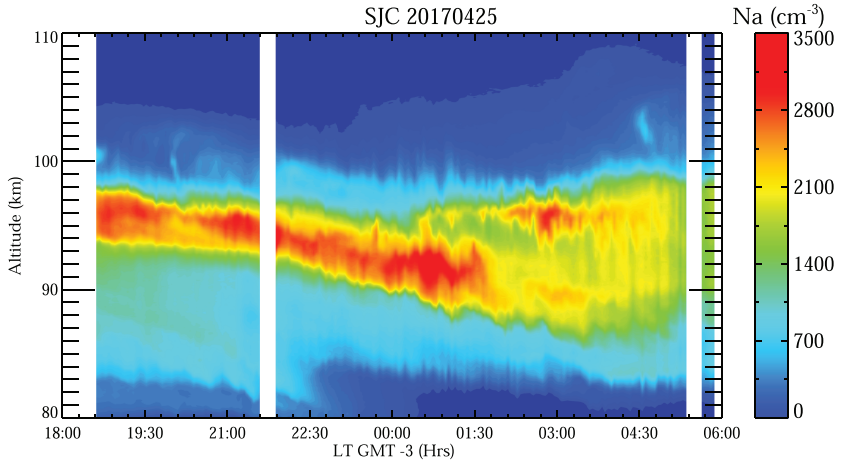

Figure 3. Height time intensity plot of Na density layer on 25 April 2017 at São José dos Campos.

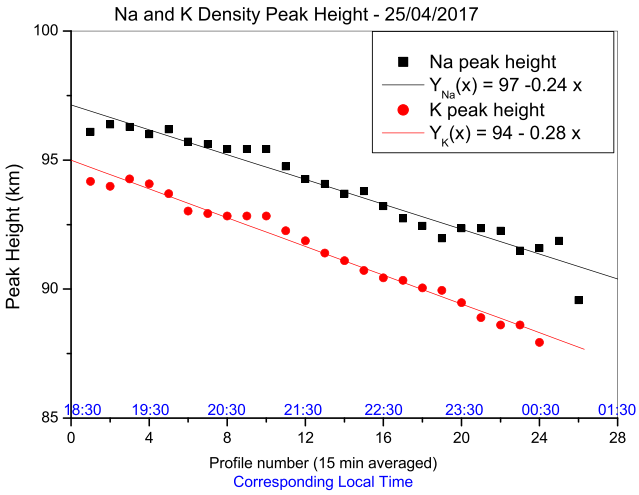

Figure 4. Peak height of both metal layers showing their time decay. Each profile number corresponds to 15 min averaged. In the *x* axis, the blue values indicate the corresponding local time to the profile number.

Plane, 1998; Delgado et al., 2006; Gerding et al., 2000; Helmer et al., 1998; Plane, 2003). Therefore, the fast downward movement of the Es layer can be the reason for the existence of Ns K layer at around 94 km at the beginning of night. Note in Figure 9b that the second Es during the first hour in which it appears has less vertical variation, with its altitude staying around 100 km at CXP and around 105 km at SJC. It is important to point out here that the Es layer does not usually get stronger during the night, as can be observed in the studies done by Resende et al. (2017) over CXP.

On these two and a half years of Na/K LIDAR data, we have seen this downward movement and bifurcation of the layers on 99 out of 152 nights of observations (66%), showing this is a common nocturnal behavior of the metal layers over SJC. This behavior and its relationship with tidal winds, gravity waves and Es has been thoroughly discussed for the normal and Ns Na layer, since the early Na measurements at SJC (e.g., Clemesha et al., 1979, 1982; Batista et al., 1985, 1989). However, no studies for K layer have been reported on this latitude. Hence, this is one of the goals for the present study, showing for the first time the characterization of nocturnal downward structures in the K layer in the Southern Hemisphere. Seasonal variation for this kind of structure is shown in Figure 10. We grouped all data observed in the same month, for example, January represents January 2017, 2018, and 2019, in other words, we build a composite year. We can see that these structures seem to occur preferentially during fall season, mainly during April. This partially agrees with the seasonal behavior of diurnal tide over CXP, a more pronounced peak around April/May, although the diurnal tide presents a second maximum around September as can be seen in Batista et al. (2004).

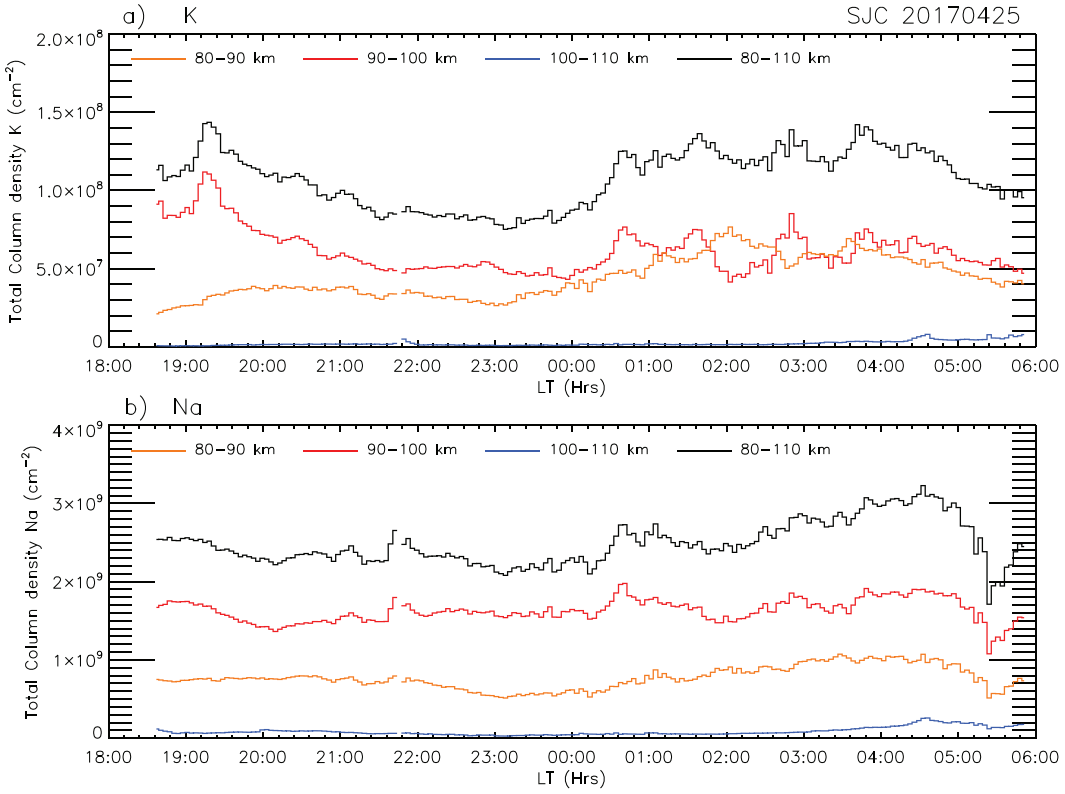

Figure 5. Total column density of K (a), and Na (b), on 25 April 2017, in different height ranges: orange line, from 80 to 90 km; red line, from 90 to 100; blue line, from 100 to 110 km; and the black line representing the total layer from 80 to 110 km high.

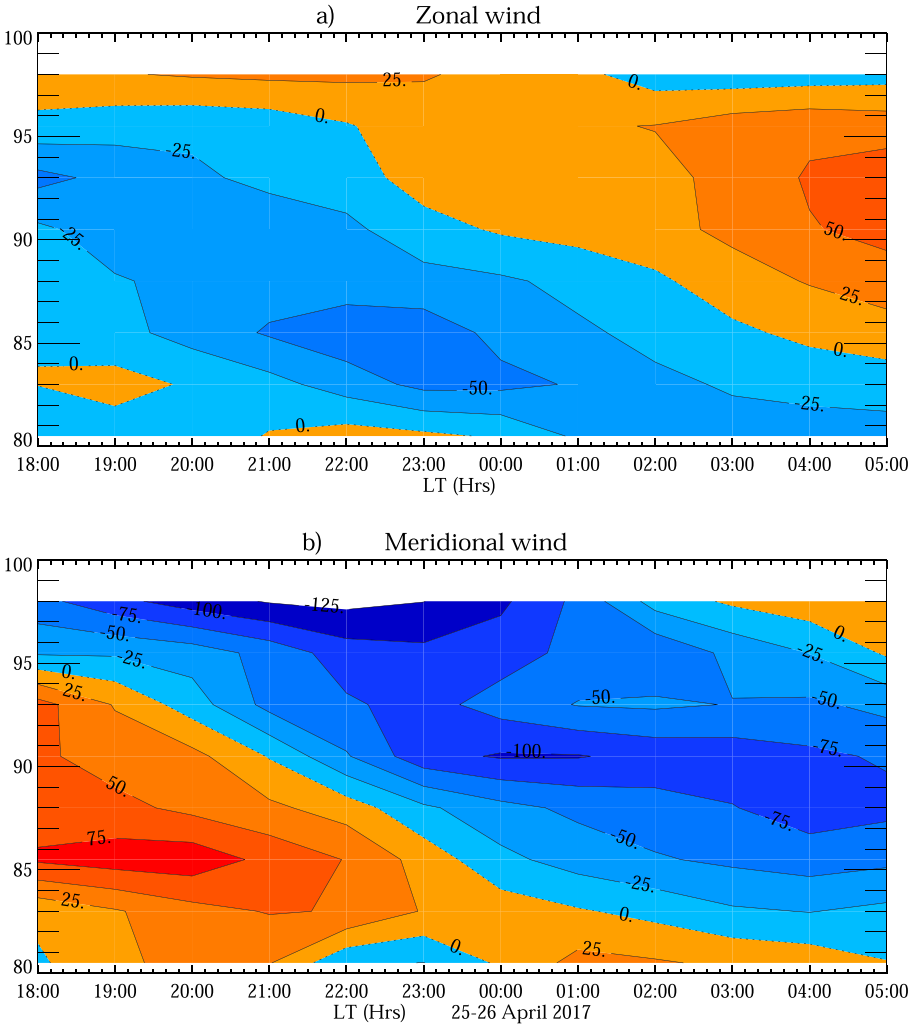

Figure 6. Zonal and Meridional wind measured by an all-sky meteor radar at Cachoeira Paulista. Blue shades indicate negative direction, that is, southward (westward) for meridional (zonal), and red shades indicate positive direction. Each contour corresponds to 25 ms^{-1}. Dotted line indicates null values of the wind.

Regarding the vertical behavior of these metal layers, we present their vertical profiles for different time averaging in Figures 11 and 12 for K and Na densities, respectively. With the aim to better characterize the vertical standard pattern of each metal layer, different time averages are taken: 3 min (individual profile = curve (a)); 1 hr (20 profiles = (curve b)); 10 hr (all night = curve (c)); 1 month (curve (d)); and 1 year (curve (e)). We can observe a bimodal characteristic on K density profiles, peaking at 86 and 96 km, either for 3 min (curve a), or for 1 hr (curve b) averages, on 25 April 2017. The all night-averaged line (c), shows a wide layer centered at around 91 km, as a result of the vertical movement of that structure. Even averaging throughout month, we still can see a remnant second peak around 96 km. However, the year averaged, curve (e) does not present any residual shape from the Ns layers. The year profile shows a full width at half maximum (FWHM) of 8.7 km and a peak height around 90 km reaching 98 atoms cm^{-3} on the peak, when applied a Gaussian fit.

For Na layer, Figure 12, we also can see the bimodal characteristic, peaking at 89 and 95 km, either for 3 min or for 1 hr averages. We can see a broad shape of the layer in the night average, probably due to remaining bimodal shape; however, this characteristic is not seen neither monthly nor yearly profiles. By Gaussian fitting, the year profile shows a FWHM of 10.6 km and a peak height around 91.8 km reaching 3,000 atoms cm^{-3} on the peak. Similar to K profiles, yearly average does not present the bimodal shape characteristic.

3.2. Seasonal Variation

In Figure 13 we can observe the seasonal variation of the monthly averaged K (panel a) and Na (panel b) densities vertical profiles measured from November 2016 to February 2019. These values correspond to

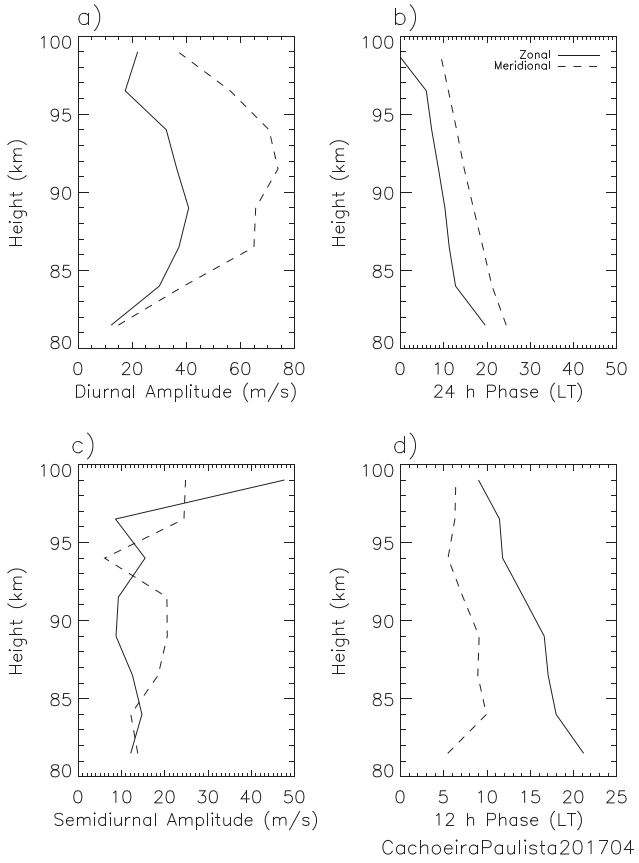

Figure 7. Monthly mean amplitudes and phases of tides observed on April 2017 over CXP by the all-sky meteor radar. The diurnal component is shown in the upper panels a) and b), and the semidiurnal component is shown in the bottom panels c) and d).

the average of all data available for each respective month. We can observe a semiannual variation with the maxima around the solstices in the K densities, being the winter maximum stronger than the summer one. This leads us to believe that K density presents also an annual variation with a maximum around wintertime, June and July. The altitude of the maximum density has small variation throughout the year and the peak averaged K density can range from 55 atoms cm^{-3} in October to ~170 atoms cm^{-3} around June/July.

Figure 13b presents the seasonal variation of Na density during the same period of observations. Semiannual variation is observed from 80 to 91 km on the Na density, with the first maximum centered on May to June and a second maximum extending from August to October. The altitude of the maximum density does not present large variation throughout year, located at around 92.5 km. On the other hand, the peak averaged Na density ranges from 1,000 atoms cm^{-3} on January up to 4,300 atoms cm^{-3} in October and can reach higher values on individual nights.

Those characteristics reported in previous paragraphs are more clearly observed in Figure 14 for K and Na, shown on the red lines and triangles and black lines and squares, respectively. This figure shows the seasonal variation of monthly averaged of K and Na column abundances, on panel (a); layer width on panel (b); and the centroid height of the layers on panel (c). These parameters were obtained by a Gaussian fit applied in the monthly averaged densities vertical profiles. Observing Na column abundance, black line, and squares in panel (a), it varies from $2x10^9$ atoms cm^{-2} around summer, to above $5x10^9$ atoms cm^{-2} in October, suggesting an annual variation with a maximum at the winter solstice. The K abundance, red line and triangles also in panel (a) (right scale), ranges from $5x10^7$ atoms cm^{-2} in April, up to $17x10^7$ atoms cm^{-2} around the winter. We can clearly note a semiannual oscillation in the abundance of K layer with maxima at the solstices. Regarding the FWHM shown on panel (b), K width varies from 8 to 11 km being around 10 km most part of the year. In the same way, Na layer width has also no large months to month variation, ranging from 11 to 14 km. Moreover, layer width varies less for Na

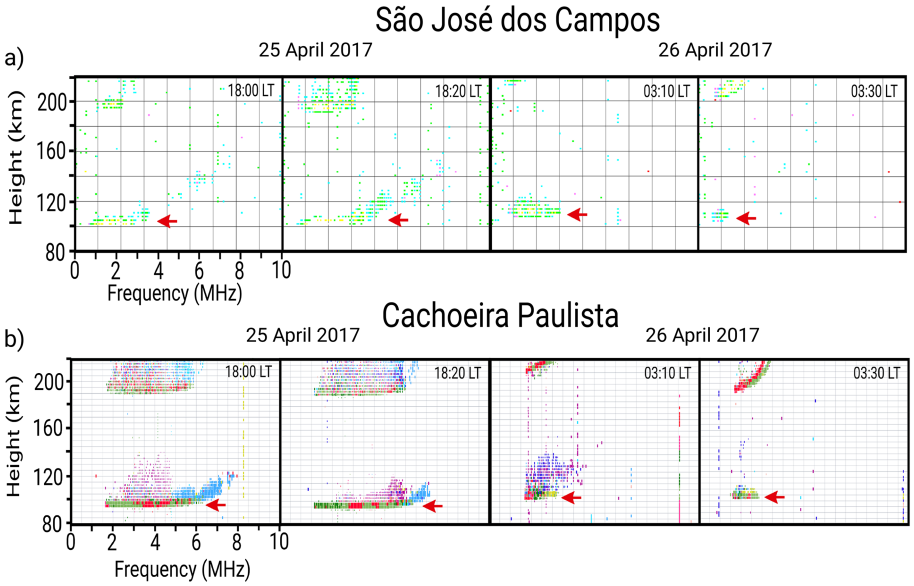

Figure 8. Ionosonde data showing a Strong Es measured simultaneously on 25 and 26 April 2017 at SJC (a), and CXP (b).

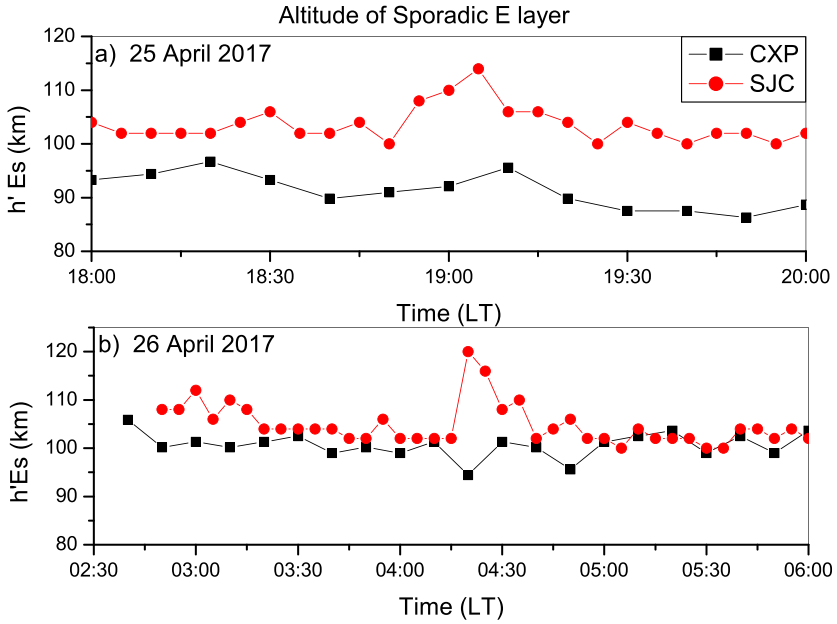

Figure 9. Altitude variation of Es layer observed by two Ionosondes on (a) 25 and (b) 26 April 2017, one at Cachoeira Paulista (CXP), black lines and squares, and at São José dos Campos (SJC), red lines and circles

than for K, and both layers reach almost the same width in March and October. On the last panel is shown the centroid height for both layers, and we can see that they have the same variation pattern, which means, both have semiannual variation with downward centroid at the solstices. Moreover, the averaged centroid of K is 90.8 km and Na is 92.3 km. Finally, we can clearly see that Na layer is wider and higher than K layer most part of the year.

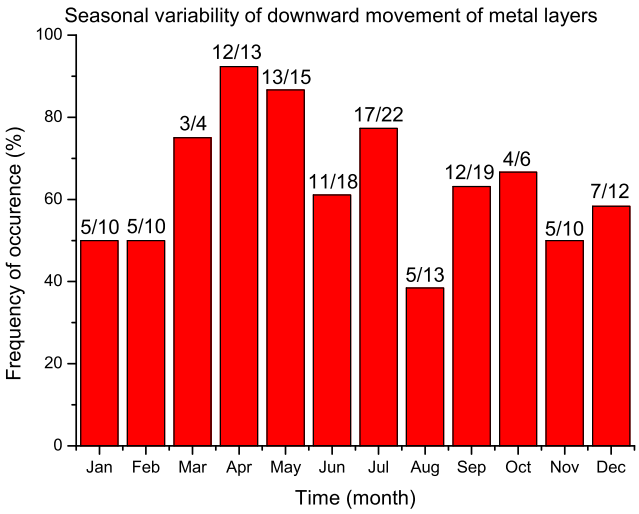

Figure 10. Seasonal variation of downward movement events measured by the new dual beam LIDAR shown in a composite year. Labels over bars represent the number of nights with downward movements over the total number of measurements in the month.

4. Discussion

4.1. Vertical Structure and Layers Characteristics

Nocturnal descending structures on Na density profiles were also observed by Simonich et al. (1979) with vertical velocity propagation between 1 to 4 km/hr also in SJC, similar to our results, and they attributed them to the dynamical effects. Moreover, they reported that the presence of this kind of descending structures showing two peak layers is present in most part of the observation. This also agrees very well with our results of 66% occurrence of these structures. The additional contribution of the present work on analyzing these structures is the simultaneous observation of Na and K layers at the same site. This allows the comparison of the behavior of these both alkali metals. The analysis of the centroid height can provide information about the mass distribution of the metal layer. Similar variation of the centroid height of different metals measured at the same site suggests that the distributions of these atoms are controlled by the same mechanism. We can observe the night evolution of peak height for Na and K layer, in Figure 4, where both show downward movement agreeing very well in the speed value. Moreover, the good correlation with the strong vertical wind shear due to tides, shown on the wind measurements at CXP suggests that the diurnal tide is acting in the nocturnal morphology of both layers. Beside the dynamical effects, we should also consider the strong Es layer occurrence at the same time, around 18:30 LT, of the Ns layer. This can guide us to the metal ion neutralization theory as a possible explanation for the Ns presence at the

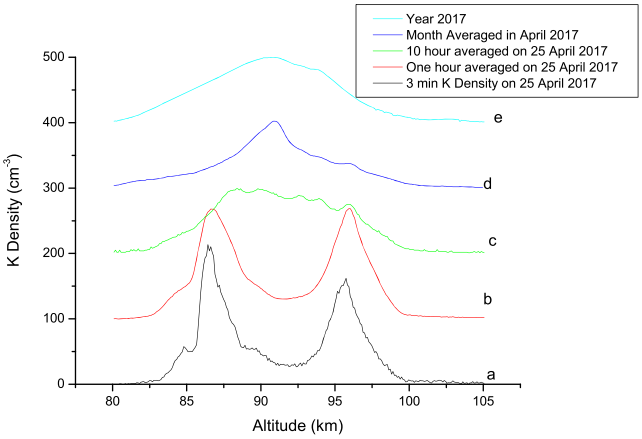

Figure 11. K profiles for different averaging time: (a) 3 min at 00:30 LT; (b) 1 hr average (from 00:00 LT to 01:00 LT); (c) 10 hr (all from 25 April 2017); (d) month of April 2017; (e) Year 2017.

beginning of the night of 25 April 2017. Delgado et al. (2012) have studied two cases of K and Ca^+ sporadic layers, high (above 100 km) and low altitude (90 to 95 km), and their connection to the chemistry and temperature dependence over Arecibo. Their results suggested that the high-altitude K Ns layer agreed very well with their chemistry modeled K Ns layer where the ion neutralization reactions for K are temperature dependent. However, their model did not reproduce very well the low-altitude K Ns layer. As their model did not consider dynamical effects, they concluded that the low-altitude Ns layer is influenced by the dynamics such as advection and wave interaction. The altitude of the K Ns layer observed in 25 April 2017 is 94 km, which is similar to the lower altitude of their study suggesting also the combination of dynamics and chemistry effects for the observations. Nevertheless, the main objective of the present work is the general behavior of the main K and Na layers; hence, we would not go deep in the discussion about the Ns layers.

In order to evaluate the nocturnal variation of production and loss of metal atoms we can analyze the total column abundance. The reason is that, an increase in the total column abundance of the neutral atoms means an input of metal atoms; this input can be a direct injection by meteor ablation, horizontal transport, or due to chemical reactions. According to the International Meteor Organization (2019), there was no meteor shower in the night of 25 April 2017. Moreover, the meteor flux observed by the meteor radar at CXP, not shown here, present the well-known diurnal variation in the meteor counting with a peak at 6:00 LT and a minimum at 18:00 LT not showing a significant relationship to the nocturnal total column abundance nor for K neither for Na. Yet the enhancements in the metal abundances observed at this night are not explained as a direct meteor injection. Because LIDAR just observe one point, we cannot correctly evaluate the importance of horizontal transport of these metal atoms. Although K and Na are both alkali metals and their chemical reactions are similar, their reactions rate coefficients are different. They are much more temperature dependent in the case of K than for Na. In this way, we show in Figure 15 the temperature data provided by SABER at 0:26 LT on 26 April 2017, over SJC. We can clearly note that the temperature at the MLT region is very disturbed at this night, showing two minima, one at ~86 km, and another at ~96 km. These two temperature minima coincide with the peak altitude of K layers following the bifurcation. Perhaps, this can explain that the total K abundance have increased about 50%, after 00:00 LT, versus only 16% of Na. Concerning the chemical reactions, we can neglect all the photochemistry reactions because our observations are during nighttime. Moreover, according to Plane et al. (2014) the energy activation for the reaction $KHCO_3 + H \rightarrow K + H_2CO_3$ is very high which make this reaction less important. Additionally, they also said that the reactions involving KO, KO_2, and KOH are temperature dependent. Yet the main chemical production of K came from the ion-neutralization through $K^+X + e^- \rightarrow K + X$ ($X = O, O_2, N_2, CO_2, H_2O$). Note that the neutralization of K and Na ions is only possible after their recombination with other neutral atmospheric elements, forming ionic cluster. Consequently, this reaction depends on the distribution of X constituents and this is dynamical dependent. Moreover, this reaction also depends on the $[K^+]$. Even though the name Es layer suggest a kind of rare event, the studies have shown that the presence of Es layer is often observed as shown in the seasonal analysis done by Resende et al. (2017). Hence, the presence of metal ions in the region of low thermosphere is often present allowing the possibility of ion-neutralization reaction.

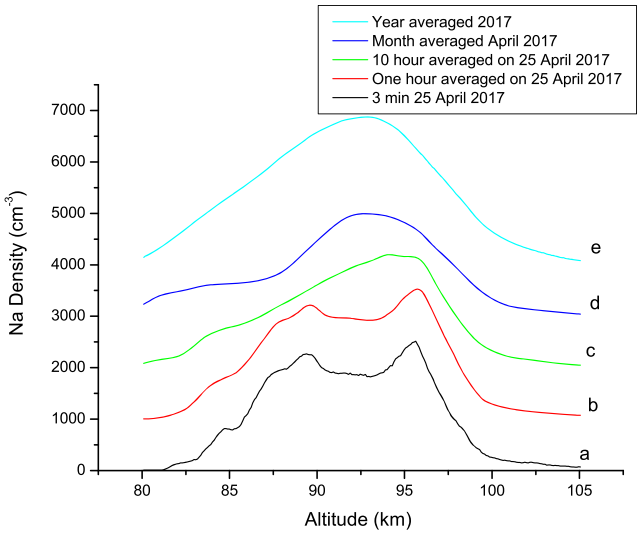

Figure 12. Same as Figure 11 but for Na profiles.

Previous works about Na and K layer characteristics obtained by LIDAR instrument are summarized on Table 1, for better comparison. Most part of K layer studies has been done in the middle and high latitudes of the Northern Hemisphere. Concerning about Na studies, there is a wide number of LIDARs for this purpose around the world. Moreover, Na layer in

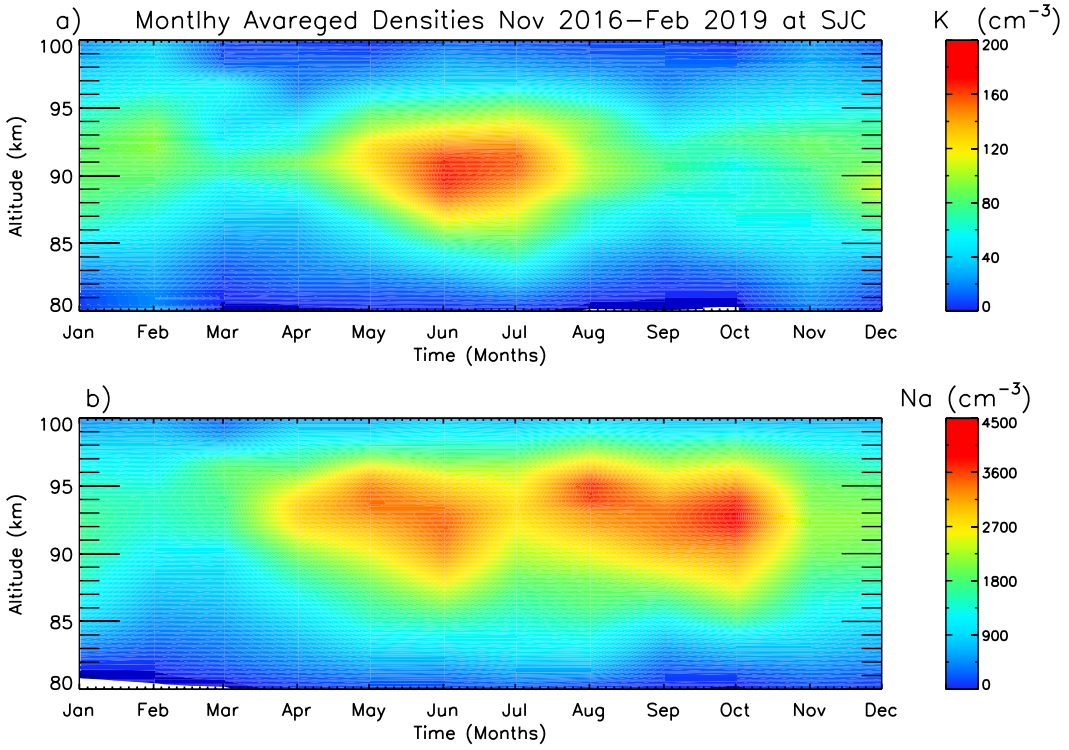

Figure 13. Seasonal variation of monthly averaged K (a) and Na (b) densities observed from November 2016 to February 2019. These values correspond to the average of all data available for each respective month.

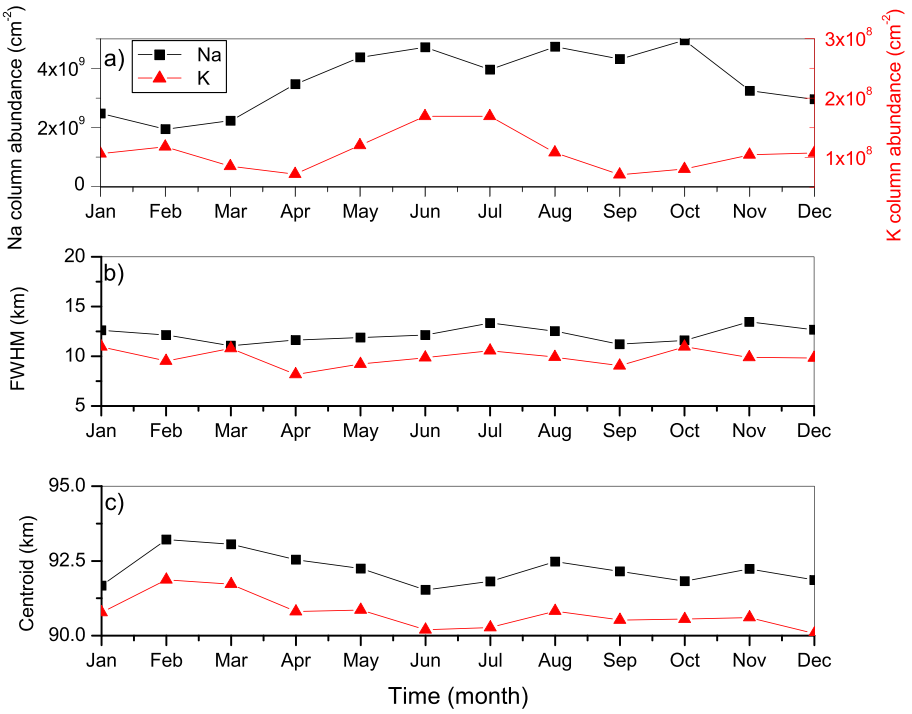

Figure 14. Monthly averaged K (red line and triangles) and Na (black line and squares) layers characteristics observed from November 2016 to February 2019. Column abundances are shown in the panel a), FWHM for both layers are shown in the panel b), and the panel c) shows the centroids of the layers.

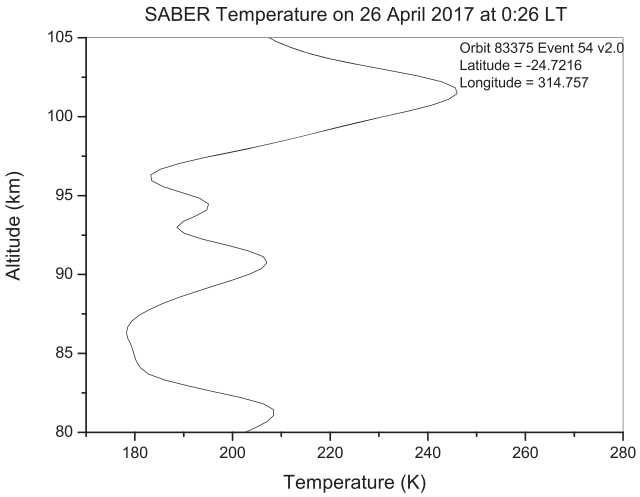

Figure 15. SABER temperature on 26 April 2017.

SJC has been studied for more than 40 years; hence, we focus our discussion in the K results. Analyzing Table 1, we can note that these metal layer characteristics have some latitudinal variation, emphasizing the importance of the present work, as this is the first study of K layer morphology at Southern Hemisphere low latitude simultaneously with Na.

Simultaneous Na and K measurements using airglow or LIDAR have shown that K peak height is below the Na layer peak (e.g., Gault & Chanin, 1974; Gault & Rundle, 1969; Megie et al., 1978), which agrees with our results. Megie et al. (1978) were the first to compare simultaneous Na and K densities measured by LIDAR, and they found that the peak K layer is about 1.2 km lower, which agrees very well with our result. Their results also showed that the Na layer is wider than the K layer, also agreeing with our results.

Von Zan and Höffner (1996) reported much lower K concentration than the values reported by Megie et al. (1978), in their measurements over Juliusruh, (54°N; 13°E) using a density and temperature LIDAR. Eska et al. (1998) analyzed 110 nights of K density profiles at a close site, Kühlungsborn, Germany (54°N, 12°E) and found the following properties of the nightly mean K layer: column density of 4.4×10^7 cm^{-2}; peak density of 47 cm^{-3}; layer centroid height of 90.5 km and root-mean-square layer width of 4.0 km, which agrees well with the results for Juliusruh.

Eska et al. (1999) showed latitudinal dependence of K column density in their observations from 71°S to 54°N using a K density and temperature LIDAR on board a cruise ship. Actually, it appears to be the first measurements of K density layer in the Southern Hemisphere. They reported that the K column density presented its large latitudinal variability in the South Hemisphere, ranging from 2.5×10^7 atoms cm^{-2}, at high latitude, up to 12×10^7 atoms cm^{-2}, close to the equator. Furthermore, the latitudinal variation of the K layer width clearly shows a broader K layer in the Southern Hemisphere during winter, ranging from 9 to 18 km, compared with the summertime Northern Hemisphere, 6–11 km. In that study, they also showed the fluctuation of the height peak density with the values oscillating between 84.7 and 92.5 km, the higher peak heights were observed in the midlatitudes for both hemispheres. Moreover, the authors observed a positive correlation between temperature and K abundance from 47°S to 8°S and from 1°N to 45°N. For better comparison with our study, we used their mean K profile with 20° Hanning filter centered at latitudes 23°S, using three nights data. As the authors reported, Ns K layers in low latitude are present in almost all days, so it becomes difficult to correctly estimate the peak altitude and the FWHM. Hence, the values presented on our Table 1 for those two variables were obtained by averaging the values from Figure 3, on their paper, respectively from panels (c) and (d), in 30°S and 10°S. We can note that even for the few nights of data between May and June their results show layer width in good agreement with our values (9–11 km vs. 6–11 km), peak height about 3 km lower (87.3 km vs. 90.9 km) and K abundance values is almost twice smaller than our results (9.5 vs. 3–20 $\times 10^7$ cm^{-2}). The Na layer characteristics are in accordance with the studies made by Simonich et al. (1979) for the same site. Simonich et al. (1979) found average layer characteristics: column density of 4.4×10^9 cm^{-2}; peak density of 3,600 cm^{-3}; layer centroid height of 94 km, and root-mean-square layer width of 13 km, which agree very well with the present results: total column abundance ranging from 1.5 to 12 $\times 10^9$ cm^{-2}; peak density 1,000–6,000 cm^{-3}; FWHM 5–19 km, and the layer centroid height of 92.3 km.

4.2. Seasonal Variation

Seasonal behavior on Na and K layers has been carried out for decades and several authors reported some differences and similarities when comparing the seasonal variation of these two alkali metal layers. The early K and Na seasonal studies reported no significant variation (Megie et al., 1978). However, posterior works pointed seasonal variation not only on column abundance but also on peak altitude and layer width (e.g., Clemesha et al., 1979). Eska et al. (1998) observed semiannual variation with maxima in summer and winter for the nightly mean column abundance and peak height K density at high latitude. Additionally, they compared the seasonal behavior of K with Na and Fe layers and found the same semiannual variation on the three metals' centroid height; however, Na and Fe showed annual variation with maximum during

Table 1
Observed Na and K Layers Characteristics by LIDAR

Author	Column density (10^7 cm^{-2})	Peak density (cm^{-3})	Layer width (km)	Peak height (K) (km)	Location
Felix et al. (1973)	9 (K)	—	—	—	18°N; 76°W
Megie et al. (1978)	30 (K) , 800 (Na)	300 (K) , 2200 (Na)	7–15 (K) 8–18 (Na)	1.2 km[a]	44° N; 6° E
Simonich et al. (1979)	440 (Na)	3600 (Na)	13.7 (Na)	94 (Na)	23°S; 46°W
Von Zahan and Höffner (1996)	4–7(K)	30–120 (K)	—	88–91 (K)	54° N; 13°E
Eska et al. (1998)	2–8 (K)	15–135 (K)	3–5 (K)	1.6 km[b]	54°N; 12°E
Eska et al. (1999)	9.5 (K)	89 (K)	9–11 (K)	87.3 km (K)	23°S
Friedman et al. (2002)	2–12 (K)	5–100 (K)	3–8 (K)	89–94 (K)	18°N; 67°W
Wang et al. (2017)	8.4 (K)	30–225 (K)	3–6 (K)	87–93 km (K)	40°N; 116°E
X. Yue, et al. (2017)	1.8–8.5 (K)	20–70 (K)	6.9 (K)	91.7 (K)	18°N; 67°W
Present work	**3–20 (K) 150–1200 (Na)**	**40–200 (K) 1000–6000 (Na)**	**6–11 (K) 5–19 (Na)**	**90.9 km (K) 92.3 km (Na)**	**23°S; 46°W**

[a]Height peak difference between Na and K layers. $Z_M(\mathrm{Na}) - Z_M(\mathrm{K})$. [b]Comparison made using Na data from Kane and Gardner (1993).

winter on their column densities instead of a semiannual variation with maxima during solstices in case of K layer. These results agree very well with ours in the results, as for the oscillation as for the timing of maxima for both Na and K layer. The annual variation on the Na column abundances with a broad maximum from equinox to equinox is also reported by Clemesha et al. (1979) and Simonich et al. (1979) over the same site. Clemesha et al. (1992) reported a sharp minimum in November over the annual variation of the centroid of Na layer at SJC. Their analysis was performed over the data obtained from 19:00 LT to 22:00 LT and excluding the Ns days. Perhaps this is the reason why we did not observe this sharp minimum on November. If we overlook the November minimum, we can observe similar semiannual variation in the Na centroid height, shown in their Figure 2.

Friedman et al. (2002) reported semiannual oscillation on the column density of K; however, no annual variation was observed on the layer width neither on layer centroid, over Arecibo (18°N, 67°W). They attributed this fact to the large frequency of Ns K layer observed in 18°N and the bimodal behavior of the K layer generally observed for May to June, which makes difficult the correct interpretation of these parameters. However, Yue et al. (2017) reported semiannual variation in the centroid height and in the column abundance for K density at the same site. The authors attributed the different results compared to the previous to the solar activity influences.

Dawkins et al. (2014) presented for the first time a near-global K and Na layers distribution from space-borne observations of resonance fluorescence in the dayglow with the total uncertainties on the densities abundance of around 15%. Their results showed that Na total layer abundance around 20°S presented an annual variation with maximum at winter while K total layer abundance presented semiannual variation with maxima in winter and summer. This agrees very well with our K results; however, those results presented by Dawkins et al. (2014) did not show the stronger maxima in the wintertime. It is important to point out that they are measuring dayglow in 10° latitude zonal means while we are measuring Na and K layer at nighttime using resonance LIDAR at a single point. Dawkins et al. (2015) compared their OSIRIS-retrieved K layer results with recently implemented K - chemical model on the Whole Atmosphere Community Climate Model (WACCM-K) (Plane et al., 2014). They showed that the large seasonal variability on K density occurs on high latitude with good agreement to the WACCM-K.

Wang et al. (2017) analyzed 2 years of K density over Beijing using a LIDAR. They reported semiannual oscillation in the column abundance and peak height with maxima in the summer and winter; also, a semiannual oscillation is clear in the centroid height with maxima in equinoxes. These results agree very well with our results.

Plane et al. (2014) presented a possible explanation for the different seasonal variations between Na and K densities. This explanation is based on two points: (1) the neutralization of K^+ ions is only favored at low temperatures during summer (North Hemisphere); and (2) cycling between K and its major neutral reservoir $KHCO_3$ is essentially temperature independent. The first argument is more relevant for high latitude, where the mesopause temperature has strong summer to winter variation. Yue et al. (2017) also discuss the temperature dependence to be the main explanation for the seasonal K behavior at low latitude. Although

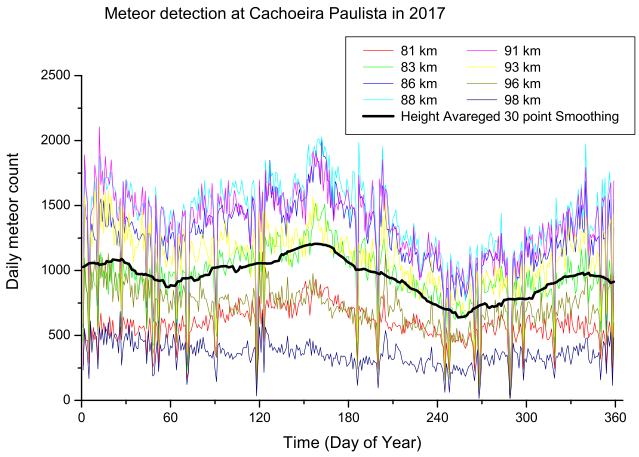

Figure 16. Seasonal variation of daily meteor echoes detected by all-sky meteor radar at CXP in 2017. The meteors were separated in eight layers of 2.5 km high, from 80 to a 100 km. Each color line corresponds to an individual height layer center at 81.25 km (red); 83.75 km (green); 86.25 km (blue); 88.75 km (light blue); 91.25 km (pink); 93.75 km (yellow); 96.25 km (dark yellow); and 98.75 km (navy). The black wider line represents the height-averaged amount using 30-point smoothing tool.

their results show negative correlation between temperature and K column abundance supporting Delgado et al.'s (2012) and Plane et al. 's (2014) conclusion, that the production of K from K^+ is favored at low temperature, they also suggest that K seasonal variability may be more significantly affected by the wave-driven transport of main reactants, such as O, CO_2, and H_2 than the K^+ ions and K through the MLT. Their results were supported by the good correlation between maxima temperature variances, suggesting gravity wave activity in the equinoxes, and the downward movement of the height centroid of the K layer.

The present work brings for the first time seasonal K density measured by LIDAR at the Southern Hemisphere. Although the Na density has been widely studied and shows a latitudinal dependence, K densities show less latitude dependence, agreeing very well with North Hemisphere high and low latitude. Takahashi et al. (1995) and Lima et al. (2018) show semiannual variation in the mesopause temperature over CXP, with minima at solstices. Even though this temperature variation agrees with Delgado et al.'s (2012) and Plane et al.'s (2014) explanation, the semiannual amplitudes in temperature fields are small, around 3 K, being not significant to support their first argument. Moreover, Gardner and Liu (2010) showed that the centroid height of the metal layers is shifted down during high gravity wave activity. Yang et al. (2010) reported semiannual variation in the temperature variances suggesting gravity wave activity over SJC being maxima during the equinoxes. Our results show that the centroid heights of the metal layers have also the semiannual variation; however, they are shifted up during the equinoxes, being the opposite.

If we compare the seasonal behavior of Na and K concentration with the meteor entrance in the upper atmosphere measured by all-sky meteor radar at CXP, Figure 16, we can see that meteors have a semiannual variation with maxima around the solstices. This partially agrees with Na and K densities behavior, which is the maximum at around May and June. However, meteors' entrance shows the second maximum around January while Na shows minimum density in this period. Moreover, the relative abundance of K to Na in the most common type of meteorites, CI chondrites, is about 8% (Mason, 1971) and for the cosmic meteors, this ratio is 6% (Grevesse & Anders, 1991). This is still a discrepancy to abundance ratio of these two alkali metals observed in this work, which is about 2.3%. However, this ratio is larger than those presented in the models, such as Eska et al. (1999) or Plane (1991, 2003), which is 1%. Nevertheless, it is important to report that the model of Eska et al. (1999) underestimates about half the K concentration for the latitude of 23°S compared with the model with observation during Polarstern campaign. Moreover, the column abundance reported by Dawkins et al. (2015) in their global climatology of K, shown on their supporting information Table S1, for 20–30°S, ranges from 2.6×10^7 atoms cm^{-2} (equinoxes) to 7.5×10^7 atoms cm^{-2} (at June solstice). These results agree in part with our results, showing the more pronounced maximum in June solstice; however, it diverges with respect to the absolute value, which is almost half of ours.

One can think that the presence of Ns layers in the Na or K layer can bias the altitude of the centroid and or the layer characteristics. Simonich et al. (2005) showed that the presence of Ns layers does not greatly affect the long-term average height distribution of atmospheric Na. This reinforces that our analysis is correctly presented.

5. Summary and Conclusion

In this work, we have analyzed more than 2 years of the new dual-beam K and Na LIDAR density over SJC. This is the first time nocturnal and seasonal analyses are presented simultaneously for K and Na layers at the Southern Hemisphere. The vertical descending structure with a rate of 1–4 km hr^{-1} and a bimodal layer seems to be a common characteristic, present on 66% of the nights observed on both metal layers. In addition, they seem to occur preferentially around April, indicating some relationship with diurnal tide that also has more pronounced maximum variation in this month observed in CXP. Although a larger temporal data series is needed in order to confirm this finding. Our results indicated that the formation of this structure is a

combination of Es layer presence, contributing with an input of new atoms by the ion-neutralization reaction, in the presence of strong wind shear at the mesopause pushing down the metal layers. This last hypothesis is supported by the similar variation of the height centroid of both K and Na layers and the good correlation with diurnal tide vertical phase speed.

The K and Na layers at 23°S show the following annual mean characteristics: The K column abundance ranges from 3 to 20 $\times$ 10^7 atoms cm^{-2}, with the layer peak around 90.9 km and width varying from 6 to 11 km. In the case of Na, the abundance varies from 15 to 120 $\times$ 10^8 atoms cm^{-2}, the peak height is around 92.3 km, and the layer width varies from 5 to 19 km. The centroid height for both metals, K and Na, present semiannual variation with maxima at the equinoxes, and the K layer is on average 1.3 km lower. The column abundance of Na layer shows general annual variation with a minimum during summer and a broad maximum almost from equinox to equinox while a semiannual variation is observed on K column abundance with maxima around the solstices. Semiannual variation is observed in both metal densities with different maxima: K shows its maxima around the solstices more pronounced around June, and Na density shows a maximum around May, and a broad one centered in September.

The very similar seasonal variation of the K layer measured in the Southern Hemisphere in comparison to the Northern Hemisphere high and low latitude, and the fact that mesopause temperature does not vary as much as that at high latitudes keep open the question about the stronger maxima at June solstice at low latitude. Moreover, seasonal variation of the meteor ablation has similar behavior of the K metal layers but not on Na variation. These all call our attention for the importance of better worldwide coverage of instruments able to monitor not only these elements but also their reactants and the physical parameters such as temperature and winds to help our understanding of chemical and dynamics in the mesopause region.

Acknowledgments
V. F. Andrioli, S. Savio, and L. C. A. Resende acknowledge China-Brazil Joint Laboratory for Space Weather and Chinese Academy of Sciences (CBJLSW) for their Postdoctoral fellowship. The authors also acknowledge CBJLSW to provide Na/K lidar data. This study was supported by NSSC research fund for key development directions, Specialized Research Fund for State Key Laboratories of China, and CBJLSW, CAS. We also thank the Brazilian National Council for Scientific and Technological Development (CNPq) for supporting scientific equipment and through the PCI program. P. R. Fagundes acknowledges FAPESP (Grant 2012/08445-9). L. C. A. Resende thanks CNPq/MCTIC (Grant 405334/2017-6). The authors would like to acknowledge the Digisonde data from CXP and CADI ionosonde data from SJC, and also a special acknowledgment to Valdir Gil Pillat for his help on the software UDIDA for CADI ionosonde data analysis. The Na/K LIDAR, CADI ionosonde data at SJC, and CXP meteor radar data, which were used in the present study, are available online at this site (http://www1.univap.br/ionosfera/Paper_Data/andrioli_jgr_2019.zip). The Digisonde data from CXP can be downloaded upon registration at the Embrace webpage from INPE Space Weather Program in the following link (http://www2.inpe.br/climaespacial/portal/en/). The SABER-measured Kinetic temperature data are available online at this site (http://saber.gats-inc.com/data_services.php).

References

Batista, P. P., Clemesha, B. R., Batista, I. S., & Simonich, D. M. (1989). Characteristics of the sporadic sodium layers observed at 23°S. *Journal of Geophysical Research*, *94*, 15,349–15,358. https://doi.org/10.1029/JA094iA11p15349

Batista, P. P., Clemesha, B. R., Simonich, D. M., & Kirchhoff, V. W. J. H. (1985). Tidal oscillations in the atmospheric sodium layer. *Journal of Geophysical Research*, *90*, 3881–3888. https://doi.org/10.1029/JD090iD02p03881

Batista, P. P., Clemesha, B. R., Tokumoto, A. S., & Lima, L. M. (2004). Structure of the mean winds and tides in the meteor region over Cachoeira Paulista, Brazil (22.7°S; 45°W) and its comparison with models. *Journal of Atmospheric and Solar-Terrestrial Physics*, *66*, 623–636.

Clemesha, B. R. (1995). Sporadic neutral metal layers in the mesosphere and lower thermosphere. *Journal of Atmospheric and Terrestrial Physics*, *57*, 725–736. https://doi.org/10.1016/0021-9169(94)00049-T

Clemesha, B. R., & Batista, P. P. (2003). Long-term variations in the centroid height of the atmospheric sodium layer. *Advances in Space Research*, *32*, 1707–1711. https://doi.org/10.1016/S0273-1177(03)90466-2

Clemesha, B. R., Batista, P. P., & Simonich, D. M. (2002). Tide-induced oscillations in the atmospheric sodium layer. *Journal of Atmospheric and Solar - Terrestrial Physics*, *64*, 1321–1325. https://doi.org/10.1016/S1364-6826(02)00115-3

Clemesha, B. R., Kirchhoff, V. W. J. H., & Simonich, D. M. (1979). Concerning the seasonal variation of the mesospheric sodium layer at low latitudes. *Planetary and Space Science*, *27*, 909–910. https://doi.org/10.1016/0032-0633(79)90019-9

Clemesha, B. R., Simonich, D. M., Batista, P. P., & Kirchhoff, V. W. J. H. (1982). The diurnal variation of atmospheric sodium. *Journal of Geophysical Research*, *87*, 181–186. https://doi.org/10.1029/JA087iA01p00181

Clemesha, B. R., Simonich, D. M., Takahashi, H., Batista, P. P., & Sahai, Y. (1992). The annual variation of the height of the atmospheric sodium layer at 23oS: Evidence for convective transport. *Journal of Geophysical Research*, *97*, 5981–5986. https://doi.org/10.1029/91JD03146

Collins, S. C., Plane, J. M. C., Kelley, M. C., Wright, T. G., Soldán, P., Kane, T. J., et al. (2002). A study of the role of ion-molecule chemistry in the formation of sporadic sodium layers. *Journal of Atmospheric and Solar - Terrestrial Physics*, *64*, 845–860. https://doi.org/10.1016/S1364-6826(02)00129-3

Cox, R. M., & Plane, J. M. C. (1998). An ion-molecule mechanism for the formation of neutral sporadic N layers. *Journal of Geophysical Research*, *103*, 6349–6359. https://doi.org/10.1029/97JD03376

Dawkins, E. C. M., Plane, J. M. C., Chipperfield, M. P., & Feng, W. (2015). The near-global mesospheric potassium layer: Observations and modeling. *Journal of Geophysical Research: Atmospheres*, *120* 7975–7987. https://doi.org/10.1002/2015JD023212

Dawkins, E. C. M., Plane, J. M. C., Chipperfield, M. P., Feng, W., Gumbel, J., Hedin, J., et al. (2014). First global observations of the mesospheric potassium layer. *Geophysical Research Letters*, *41*, 5653–5661. https://doi.org/10.1002/2014GL060801

Delgado, R., Friedman, J. S., Fentzke, J. T., Raizada, S., Tepley, C. A., & Zhou, Q. (2012). Sporadic metal atom and ion layers and their connection to chemistry and thermal structure in the mesopause region at Arecibo. *Journal of Atmospheric and Solar-Terrestrial Physics*, *74*(1364-6826), 11–23. https://doi.org/10.1016/j.jastp.2011.09.004

Delgado, R., Weiner, B. R., & Friedman, J. S. (2006). Chemical model for mid-summer lidar observations of mesospheric potassium over the Arecibo Observatory. *Geophysical Research Letters*, *33*, L02801. https://doi.org/10.1029/2005GL024326

Eska, V., Hoffner, J., & von Zahn, U. (1998). Upper atmosphere potassium layer and its seasonal variations at 54°N. *Journal of Geophysical Research*, *103*(A12), 29,207–29,229, 214. https://doi.org/10.1029/98JA02481

Eska, V., von Zahn, U., & Plane, J. M. C. (1999). The terrestrial potassium layer (75–110 km) between 71°S and 54°N: Observations and modeling. *Journal of Geophysical Research*, *104*, 17,173–17,186. https://doi.org/10.1029/1999JA900117

Felix, F., Keenliside, W., Kent, G., & Sandford, M. C. W. (1973). Laser radar observations of atmospheric potassium. *Nature*, *246*(5432), 345–346. https://doi.org/10.1038/246345a0

Friedman, J. S., Collins, S. C., Delgado, R., & Castleberg, P. A. (2002). Mesospheric potassium layer over the Arecibo Observatory, 18.3°N 66.75°W. *Geophysical Research Letters*, *29*(5), 1071. https://doi.org/10.1029/2001GL013542

Gardner, C. S., & Liu, A. Z. (2010). Wave-induced transport of atmospheric constituents and its effect on the mesospheric Na layer. *Journal of Geophysical Research*, *115*, D20302. https://doi.org/10.1029/2010JD01414

Gault, W. A., & Chanin, M. L. (1974). Twilight potassium at Haute-Provence. *Annales Geophysicae*, *30*, 369–373. https://doi.org/10.1139/p69-011

Gault, W. A., & Rundle, H. N. (1969). Twilight observations of upper atmospherics sodium, potassium and lithium. *Canadian Journal of Physics*, *47*, 85–98. https://doi.org/10.1139/p69-011

Gerding, M., Alpers, M., Zahn, U.v., Rollason, R. J., & Plane, J. M. C. (2000). Atmospheric Ca and Ca+ layers: Midlatitude observations and modeling. *Journal of Geophysical Research*, *105*, 27,131–27,146. https://doi.org/10.1029/2000JA900088

Grevesse, N., & Anders, E. (1991). Solar element abundances. In *Solar Interior and Atmosphere* (pp. 1227–1234). Tucson: Univ. of Ariz. Press.

Helmer, M., Plane, J. M. C., Quian, J., & Gardner, C. S. (1998). A model of meteoric iron in the upper atmosphere. *Journal of Geophysical Research*, *103*, 10,913–10,926. https://doi.org/10.1029/97JD03075

International meteor organization (2019). Meteor shower in 2017 accessed by: http://press.exoss.org/wp-content/uploads/2016/12/Calendario-Exoss-Chuva-Meteoros-2017.pdf. Accessed on June 12, 2019.

Jiao, J., Yang, G., Cheng, X., Liu, Z., Wang, J., Yan, Z., et al. (2017). Simultaneous lidar observation of peculiar sporadic K and Na layers at São José dos Campos (23.1°S, 45.9°W), Brazil. *Advances in Space Research*. https://doi.org/10.1016/j.asr.2017.12.002

Jiao, J., Yang, G., Wang, J., Cheng, X., Li, F., Yang, Y., et al. (2015). First report of sporadic K layers and comparison with sporadic Na layers at Beijing, China (40.6°N, 116.2°E). *Journal of Geophysical Research: Space Physics*, *120*, 5214–5225. https://doi.org/10.1002/2014JA020955

Kane, T. J., & Gardner, C. S. (1993). Structure and seasonal variability of the nighttime mesospheric Fe layer at midlatitudes. *Journal of Geophysical Research*, *98*, 16,875–16,886. https://doi.org/10.1029/93JD01225

Kirchhoff, V. W. J. H., & Clemesha, B. R. (1973). Atmospheric Sodium Measurements at 23 S. *Journal of Atmospheric and Terrestrial Physics*, *35*, 1493–1495.

Lima, L. M., Batista, P. P., & Paulino, A. R. (2018). Meteor radar temperatures over the Brazilian low-latitude sectors. *Journal of Geophysical Research: Space Physics*, *123*, 7755–7766. https://doi.org/10.1029/2018JA025620

MacDougall, J. W., Grant, I. F., & Shen, X. (1995). The Canadian advanced digital ionosonde: design and results, Report UAG-14: Ionospheric Networks and Stations. World Data Center A for Solar-Terrestrial Physics, 21-27.

Mason, B. (1971). *Handbook of elemental abundances in meteorites*. Newark, NJ: Gordon and Breach.

Megie, G., Bos, F., Blamont, J. E., & Chanin, M. L. (1978). Simultaneous nighttime lidar measurements of atmospheric sodium and potassium. *Planetary and Space Science*, *26*, 27–35. https://doi.org/10.1016/0032-0633(78)90034-X

NRLMSISE-00 (2017). https://ccmc.gsfc.nasa.gov/cgi-bin/modelweb/models/vitmo_model.cgi Accessed on 13/02/2017.

Pimenta, A. A., Clemesha, B. R., Simonich, D. M., & Batista, P. P. (2004). Morphology of the mesospheric sodium layer and its relation with gravity wave perturbations. In G. Pappalardo, & A. Amodeo (Eds.), *22nd International Laser Radar Conference (ILRC)* (pp. 625–627). Noordwijk, Netherlands, Matera, Italy: Esa Publications Division C/O Estec, Po Box 299, 2200 Ag.

Plane, J. M. C. (1991). The chemistry of meteoric metals in the Earth's upper atmosphere. *International Reviews in Physical Chemistry*, *10*, 55–106. https://doi.org/10.1080/01442359109353254

Plane, J. M. C. (2003). Atmospheric chemistry of meteoric metals. *Chemical Reviews*, *103*(12), 4963–4984. https://doi.org/10.1021/cr0205309

Plane, J. M. C., Feng, W. F., & Dawkins, E. (2015). The Mesosphere and Metals: Chemistry and Changes. *Chemical Reviews*, *115*(10), 4497–4541. https://doi.org/10.1021/cr500501m

Plane, J. M. C., Feng, W., Dawkins, E., Chipperfield, M. P., Höffner, J., Janches, D., & Marsh, D. R. (2014). Resolving the strange behavior of extraterrestrial potassium in the upper atmosphere. *Geophysical Research Letters*, *41*, 4753–4760. https://doi.org/10.1002/2014GL060334

Reinisch, B. W. (1986). New techniques in ground-based ionospheric sounding and studies. *Radio Science*, *21*(3), 331–341.

Resende, L. C. A., Batista, I. S., Denardini, C. M., Batista, P. P., Carrasco, A. J., Andrioli, V. F., & Moro, J. (2017). Simulations of blanketing sporadic *E*-layer over the Brazilian sector driven by tidal winds. *Journal of Atmospheric and Solar-Terrestrial Physics*, *154* (ISSN 1364-6826), 104–114. https://doi.org/10.1016/j.jastp.2016.12.012

Simonich, D. M., Clemesha, B. R., & Batista, P. P. (2005). Sporadic sodium layers and the average vertical distribution of atmospheric sodium. *Advances in Space Research*, *35*(11), 1976–1980. https://doi.org/10.1016/j.asr.2005.06.030

Simonich, D. M., Clemesha, B. R., & Kirchhoff, V. W. J. H. (1979). The mesospheric sodium layer at 23 S: Nocturnal and seasonal variations. *Journal of Geophysical Research*, *84*, 1543–1550. https://doi.org/10.1029/JA084iA04p01543

Slipher, V. M. (1929). Emission in the spectrum of the light of the night sky. *Publications of the Astronomical Society of the Pacific*, *41*, 262–263.

Sullivan, H. M., & Hunten, D. M. (1962). Relative abundance of lithium, sodium and potassium in the upper atmosphere. *Nature*, *195*(4841), 589–590. https://doi.org/10.1038/195589a0

Swider, W. (1987). Chemistry of mesospheric potassium and its different seasonal behavior as compared to sodium. *Journal of Geophysical Research*, *92*, 5621–5626. https://doi.org/10.1029/JD092iD05p05621

Takahashi, H., Clemesha, B. R., & Batista, P. P. (1995). Predominant semi-annual oscillation of the upper mesospheric airglow intensities and temperatures in the equatorial region. *Journal of Atmospheric and Terrestrial Physics*, *57*, 407–414. https://doi.org/10.1016/0021-9169(94)E0006-9

von Zahn, U., & Höffner, J. (1996). Mesopause temperature profiling by potassium lidar. *Geophysical Research Letters*, *23*(2), 141–144. https://doi.org/10.1029/95GL03688

Wang, Z., Yang, G., Wang, J., Yue, C., Yang, Y., Jiao, J., et al. (2017). Seasonal variations of meteoric potassium layer over Beijing (40.41°N, 116.01°E). *Journal of Geophysical Research: Space Physics*, *122*, 2106–2118. https://doi.org/10.1002/2016JA023216

Yang, G., Clemesha, B., Batista, P., & Simonich, D. (2010). Seasonal variations of gravity wave activity and spectra derived from sodium temperature lidar. *Journal of Geophysical Research*, *115*, D18104. https://doi.org/10.1029/2009JD012367

Yue, X., Friedman, J. S., Wu, X., & Zhou, Q. H. (2017). Structure and seasonal variations of the nocturnal mesospheric K layer at Arecibo. *Journal of Geophysical Research: Atmospheres*, *122*, 7260–7275. https://doi.org/10.1002/2017JD026541

Yue, X., Zhou, Q., Yi, F., Friedman, J., Raizada, S., & Tepley, C. (2016). Simultaneous and common-volume lidar observations of K/Na layers and temperature at Arecibo Observatory(18°N, 67°W). *Journal of Geophysical Research: Atmospheres*, *121*, 8038–8054. https://doi.org/10.1002/2015JD024494

Zhou, Q., Friedman, J., Raizada, S., Tepley, C., & Morton, Y. T. (2005). Morphology of nighttime ion, potassium and sodium layers in the meteor zone above Arecibo. *Journal of Atmospheric and Terrestrial Physics*, *67*, 1245–1257. https://doi.org/10.1016/j.jastp.2005.06.013

Zhou, Q., Raizada, S., Tepley, C. A., & Plane, J. M. C. (2008). Seasonal and diurnal variation of electron and iron concentrations at the meteor heights above Arecibo. *Journal of Atmospheric and Solar - Terrestrial Physics*, *70*, 49–60. https://doi.org/10.1016/j.jastp.2007.09.012